water

MDPI

Article

Hydrological and Geochemical Modeling of Water Availability and Quality in the Jordan Valley Under Climate Change

Antonia Maragkaki [1,*], Sofia D. Nerantzaki [2], Anan Jayyousi [3], Suleiman Halasah [4], Abeer Albalawneh [5], Luma Hamdi [5], Maria A. Lilli [1], Dionissis Efstathiou [1], Maram Al Naimat [5], Safaa Al Jaafreh [5] and Nikolaos P. Nikolaidis [1]

[1] Hydrogeochemical Engineering and Remediation of Soils Laboratory, School of Chemical and Environmental Engineering, Technical University of Crete, 73100 Chania, Greece; mlilli@tuc.gr (M.A.L.); diefstathiou@tuc.gr (D.E.); ninikolaidis@tuc.gr (N.P.N.)
[2] School of Mineral Resources Engineering, Technical University of Crete, 73100 Chania, Greece; snerantzaki@tuc.gr
[3] Architectural and Civil Engineering Division, Center for Energy, Water, and Food Security Research, An-Najah National University, Nablus P.O. Box 707, Palestine; anan@najah.edu
[4] Green Spectrum for Environmental Consulting, Amman 77110, Jordan; suleiman.halasah@gmail.com
[5] National Agricultural Research Center, P.O. Box 639, Baqa 19381, Jordan; aberfer@yahoo.com (A.A.); lumahamdi21@yahoo.com (L.H.); maramjameel80@gmail.com (M.A.N.); safabj@yahoo.com (S.A.J.)
* Correspondence: amaragkaki1@tuc.gr

Abstract

The Jordan Valley is a heavily modified, data-limited transboundary river basin where water availability is constrained by both climate conditions and intensive human intervention. This study applies an integrated hydrological and hydrogeochemical modeling framework using the Soil and Water Assessment Tool (SWAT) to quantify basin-scale water availability and quality and to assess climate change impacts for the period 2000–2021. Results indicate that the basin is strongly evapotranspiration-dominated, with mean annual precipitation of 298.9 mm and precipitation-derived evapotranspiration accounting for 66.3% of rainfall. When externally supplied irrigation water is included, total evapotranspiration increases markedly, highlighting the strong dependence of agriculture on imported surface water and groundwater abstractions. Only a small fraction of total water input contributes to river discharge toward the Dead Sea, indicating a very limited internal water surplus. Hydrological dynamics are largely controlled by upstream dams and transboundary diversions, while nitrate and sediment simulations demonstrate a close coupling between hydrology, land use, and water quality. Climate projections suggest further reductions in water availability during the 21st century, exacerbating existing water scarcity. Overall, the study illustrates how intensive regulation and irrigation dependency constrain water availability in the Jordan Valley and in similar heavily modified transboundary river basins.

Keywords: hydrological budget; SWAT; transboundary river basin; irrigation dependency; climate projections

Academic Editor: Fang Yenn Teo

Received: 29 January 2026
Revised: 10 March 2026
Accepted: 17 March 2026
Published: 19 March 2026

1. Introduction

The Jordan Valley (JV) is a critical transboundary region in the Eastern Mediterranean, playing a central role in agricultural production, food security, economic development, and ecosystem sustainability in Jordan and Palestine [1]. However, this role is increasingly threatened by climate change, which exacerbates already scarce water resources and intensifies socio-economic pressures. Rising temperatures, altered precipitation regimes, and

more frequent extreme events directly affect water availability, agricultural productivity, and ecosystem stability [2–4]. The Eastern Mediterranean is recognized as a climate change hotspot [5,6], and regional climate projections indicate declining precipitation and increasing evapotranspiration across the Jordan River basin, reinforcing expectations of growing hydroclimatic stress.

In parallel, the hydrological regime of the Jordan Valley has been heavily modified by dams, reservoirs, pumping stations, and large-scale water transfers, resulting in reduced downstream inflows, increased salinity, and deteriorating water quality [7–10]. Overexploitation of groundwater, combined with pollution from agrochemicals and untreated wastewater, further constrains both water quantity and quality [9,11,12]. Hydrochemical investigations have clarified salinity sources and groundwater–surface water interactions in the Lower Jordan system. For instance, previous studies [13,14] identified the combined influence of saline groundwater discharge, agricultural return flows, and wastewater inputs, while other investigations [15] traced deep evaporated brines affecting groundwater systems. Although these studies substantially improved process understanding, they did not provide integrated basin-scale simulations linking hydrological dynamics with water quality evolution.

At the groundwater scale, physically based numerical models have been applied under data-scarce semi-arid conditions. Previous modeling studies [16,17] demonstrated the feasibility of simulating groundwater flow in sub-catchments of the Lower Jordan Valley using three-dimensional and meso-scale hydrological modeling approaches. However, these efforts were spatially limited and not dynamically coupled with surface water routing or nutrient transport at the valley scale.

Management-oriented tools have also been employed. Water allocation analyses based on integrated water management frameworks [18] and irrigation deficit assessments [19] explored water distribution under climate variability, while remote sensing–based water accounting approaches [20] improved estimates of agricultural water consumption. Nevertheless, these approaches primarily address sectoral allocation and demand management rather than physically based coupling of surface water, groundwater, and hydrogeochemical processes.

Internationally, integrated modeling frameworks increasingly emphasize dynamic coupling between hydrological compartments. Recent studies [21] demonstrated the benefits of linking SWAT and MODFLOW to simulate bidirectional surface–groundwater exchange, while other model developments [22] have incorporated aboveground and subsurface anthropogenic impacts into distributed hydrological modeling frameworks. Additional work [23] extended SWAT to represent groundwater quality parameters such as nitrate and total dissolved solids. Systematic reviews [24] and climate-focused assessments [25] highlight the growing use of integrated hydrological models under land use and climate change scenarios, yet also underline that simultaneous quantity–quality assessments in semi-arid basins remain comparatively limited. However, comparable integrated basin-scale applications remain absent for the Jordan Valley. Recent methodological advances have also emphasized the value of combining computationally efficient surrogate models with global sensitivity analysis to diagnose dominant controls in complex hydro-biogeochemical systems, thereby improving process interpretation under strong uncertainty; this broader development further supports the use of structured, process-based modeling frameworks in data-limited environmental applications [26].

In the Jordan Valley, modeling efforts remain fragmented, typically addressing either surface water [7,8,27] or localized groundwater processes [9,12], without valley-scale integration of surface–groundwater interactions and nutrient dynamics under combined land use and climate change scenarios. This lack of an integrated, basin-scale modeling

framework limits the ability to quantitatively assess future water availability and quality under evolving environmental pressures.

To address this gap, this study applies the Soil and Water Assessment Tool (SWAT), implemented through QSWAT, to simulate the coupled hydrological and hydrogeochemical response of the Jordan Valley. The model is calibrated and validated against available hydrological data to ensure a robust representation of basin processes. The framework quantifies the basin-scale water balance and evaluates the combined impacts of land-use management practices and climate change scenarios on both surface and groundwater quantity and quality. Particular emphasis is placed on explicit simulation of the nitrogen cycle as an indicator of agricultural and livestock pressures. By integrating surface water, groundwater recharge, and nutrient transport within a unified modeling approach, this study provides a quantitative basis for adaptive water management in one of the most water-stressed regions of the Eastern Mediterranean [3,5,28,29]. To our knowledge, this represents the first basin-scale application in the Jordan Valley that simultaneously integrates surface water processes, groundwater recharge dynamics, and nitrogen transport under combined land-use management and CMIP6 climate change scenarios.

2. Materials and Methods

2.1. Study Area

The study area includes the Jordanian, Israeli, and Palestinian sectors of the Jordan Valley, extending along both margins of the Rift Depression from Lake Tiberias in the north to the Dead Sea in the south. The valley is approximately 104 km long and 4–16 km wide, covering 2917 km^2, of which 1343 km^2 lie on the eastern side and 1574 km^2 on the western side, based on QSWAT watershed delineation. Elevations range from about 250 m above sea level to 419 m below sea level at the Dead Sea.

The climate shifts from semi-arid in the north to arid in the south, with hot summers and mild winters. Mean annual precipitation decreases from about 400 mm in the north to roughly 180 mm in the south [1]. Long-term observations from the North Ghor and Mid Ghor stations indicate a decline in rainfall of 11% and 34%, respectively, between 1982 and 2021 [3,4,7], accompanied by an increase of approximately 1.9 °C in mean annual temperature [4]. These trends are consistent with regional projections identifying the Eastern Mediterranean as a climate change hotspot [6,30].

The hydrological regime is strongly influenced by upstream regulation and transboundary water management. Reported inventories indicate more than ~45 dams (≈390 MCM total capacity), extensive groundwater abstraction, and major water transfers—most notably from Lake Tiberias via the Israeli National Water Carrier—have substantially reduced inflows to the Lower Jordan River and the Dead Sea [7–10]. Additional pressures arise from distribution losses, agricultural return flows, and pollution from agrochemicals and untreated wastewater [9,11,12]. The Dead Sea water level has been declining at a rate exceeding one meter per year [7,11]. Because the Jordan Valley is a transboundary and highly regulated system with fragmented monitoring and inconsistent reporting across jurisdictions, commonly cited basin statistics (e.g., dam inventories/capacities, distribution losses, abstraction/diversion volumes) should be interpreted as indicative values; reported figures vary by source, reporting year, and definition.

Geologically, the basin consists mainly of unconsolidated alluvial deposits with basalt outcrops in the north [31,32]. Dominant soil types include Calcisols, Fluvisols, and Vertisols, reflecting the geomorphological evolution of the Rift system. Land use is heterogeneous, with agriculture covering approximately 32% of the area, alongside forests, pastures, urban zones, wadies, reservoirs, and aquaculture facilities.

Figure 1 presents the spatial configuration of the watershed, including land use, soil distribution, SWAT subbasins, stream reaches, and key hydrological monitoring locations.

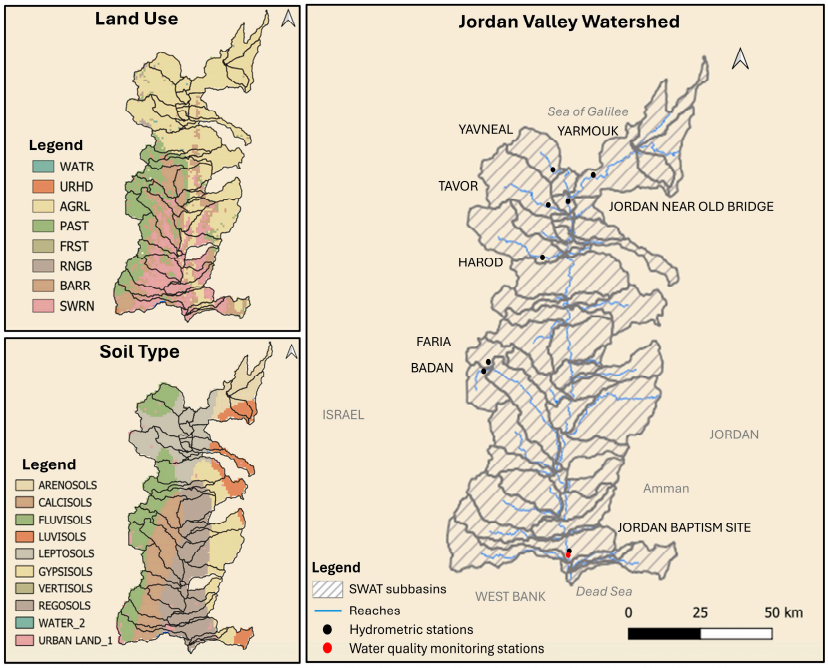

Figure 1. Land use, soil types, and hydrological features of the Jordan Valley Watershed, including subbasins delineated using the Soil and Water Assessment Tool (SWAT) implemented through QSWAT (version 2.0.1).

2.2. Modeling Framework Overview

This study applies the Soil and Water Assessment Tool (SWAT) to simulate hydrological processes, nutrient transport, and sediment dynamics in the Jordan Valley Watershed under historical and projected climate conditions. The modeling framework integrates watershed delineation and model setup, hydrological calibration and model evaluation, geochemical and sediment transport modeling, and climate change impact assessment.

SWAT (Soil and Water Assessment Tool; USDA-ARS, Temple, TX, USA) was implemented through the QSWATinterface (version 2.0.1) within QGIS (version 3.34.11-Prizren; Open-Source Geospatial Foundation, Beaverton, OR, USA) and parameterized using high-resolution topographic, land use, soil, and meteorological datasets. Model calibration and evaluation were conducted using observed streamflow, nitrate, and suspended sediment data from key monitoring locations within the basin. Future climate impacts were assessed using bias-corrected projections from multiple CMIP6 global climate models under different emission scenarios. Model performance was evaluated using the Nash–Sutcliffe Efficiency (NSE), log-transformed Nash–Sutcliffe Efficiency (log-NSE), Kling–Gupta Efficiency (KGE), coefficient of determination (R^2), and percent bias (PBIAS) to assess the reliability and robustness of the simulated hydrological and water-quality processes [33,34].

2.3. SWAT Model Setup

Hydrological modeling was conducted using QSWAT (version 2.0.1), a GIS (Geographic Information System)-based interface for the Soil and Water Assessment Tool (SWAT), implemented within QGIS (version 3.34.11-Prizren; Open-Source Geospatial Foundation, Beaverton, OR, USA). The study basin was subdivided into sub-catchments and further into Hydrological Response Units (HRUs), each characterized by unique combinations of land use, soil type, and slope. This hierarchical structure allows the model to capture spatial variability in hydrological processes.

Model inputs included a Digital Elevation Model (DEM), land use and soil maps, and daily meteorological data, including precipitation and temperature. Precipitation data were obtained from stations operated by the Israel Meteorological Service (IMS) and the Center for Hydrometeorology and Remote Sensing (CHRS), while temperature data were obtained from stations operated by the Israel Meteorological Service (IMS), the National Agricultural Research Center (NARC), the Water Authority of Jordan (WAJ), and NASA [35]. Climate Forecast System Reanalysis (CFSR) data were used to provide additional meteorological variables required by the SWAT model, including solar radiation, relative humidity, and wind speed. Hydrological flow records from gauging stations along the Jordan River and its tributaries were used for calibration.

High-resolution geospatial data supported the model setup. The DEM was sourced from the Shuttle Radar Topography Mission (SRTM GL1, 2000) at 30 m resolution, providing detailed elevation information [35]. Land use data were obtained from FAO GLC-SHARE, offering a comprehensive global land cover classification [36]. Soil information was derived from the Harmonized World Soil Database version 2.0 (HWSD v2.0), ensuring consistent and harmonized global soil coverage [37].

2.4. Hydrological Modeling

SWAT calibration was performed using observed daily discharge data from hydrometric stations distributed across the Jordan Valley. The selected stations represent key upstream, midstream, and downstream locations of the Jordan River system and its major tributaries.

The geographic coordinates (latitude, longitude; WGS84) of the monitoring stations are as follows: Yavneal (32.697363° N, 35.558599° E), Tavor (32.607050° N, 35.544820° E), Harod (32.506477° N, 35.518539° E), Jordan Near Old Bridge (32.624565° N, 35.562990° E), Jordan Baptism Site (31.837247° N, 35.546633° E), Yarmouk (32.685505° N, 35.636677° E), Faria (32.263928° N, 35.352043° E) and Badan (32.261216° N, 35.351047° E). Observed discharge data were available for the following stations and periods: Yavneal (2013–2019), Jordan Near Old Bridge (2013–2017), Tavor (2011–2015), Jordan Baptism Site (2012–2021), Harod (2000–2021), Faria (2004–2007), Badan (2004–2007) and Yarmouk (2000–2020). The discharge data for Yavneal, Jordan; Near Old Bridge, Tavor, Jordan; Baptism Site, Harod; and Yarmouk were obtained from the Hydrological Service of Israel, part of the Israel Water Authority, while data for the Faria and Badan stations were provided by An-Najah National University (Nablus, Palestine). These datasets were used as input for model calibration and model evaluation at a daily time step.

Because most station records were short and discontinuous, a formal split-sample calibration–validation procedure was not feasible for the full network. The SWAT model was configured to simulate hydrological processes at daily and monthly temporal resolutions, including streamflow, evapotranspiration, surface runoff, and infiltration.

Model performance was evaluated using the Nash–Sutcliffe Efficiency (NSE), log-transformed Nash–Sutcliffe Efficiency (log-NSE) since our main concern is capturing the base flow, Kling–Gupta Efficiency (KGE), which is useful when base flow recession curves and timing and volume matter, coefficient of determination (R^2), and percent bias (PBIAS), following [34].

Parameter calibration and global sensitivity analysis were performed with SWAT-CUP using the Sequential Uncertainty Fitting algorithm (SUFI-2) [38,39]. The most sensitive hydrological parameters were identified through Latin Hypercube Sampling and multiple regression analysis. Twenty-two parameters (Supplementary Table S1) were adjusted within ±90% of their baseline values, resulting in 660 simulations per sub-basin.

2.5. Geochemical and Sediment Transport Modeling

Geochemical and sediment transport calibration of SWAT focused on reproducing observed nitrate and suspended sediment concentrations at the Jordan Baptism Site monitoring location (approximate coordinates: 31.837° N, 35.547° E), situated in the lower Jordan River reach near the outlet to the Dead Sea. As the exact coordinates are not specified in the original publications, the monitoring location was approximated based on the documented site description. Calibration was based on daily observations of nitrate (mg/L NO_3^-) and suspended sediment concentration (turbidity in mg/L) reported by [14], which represents the only available long-term, high-frequency water-quality dataset for the lower Jordan River, based on the literature review. These observations provide an integrated measure of nutrient and sediment export from the basin, reflecting upstream hydrological, agricultural, and geomorphological processes. Because continuous, basin-wide water-quality observations were unavailable, nitrate and sediment calibration primarily constrained outlet-integrated behavior at the Jordan Baptism Site; therefore, simulated upstream spatial patterns should be interpreted as model-based hypotheses rather than independently validated spatial estimates.

Nitrate loads from agricultural and livestock sources were estimated using a standard mass-balance approach based on regional agricultural statistics, crop distributions, and fertilizer application rates. Livestock nitrogen inputs were derived from animal population data combined with species-specific nitrogen excretion coefficients reported in internationally accepted sources [40–43]. These coefficients represent typical manure production and nitrogen content for major livestock categories and are consistent with values reported in the Hellenic Code of Good Agricultural Practices and national agricultural guidelines.

For sediment calibration, the elevated sediment concentrations observed in the field at the Jordan Baptism Site [14] indicated the need to adjust model parameters in a manner that increases simulated sediment yield. In SWAT, sediment concentrations are primarily governed by parameters associated with hillslope erosion and channel sediment dynamics. Key hillslope parameters include support practice factor (USLE_P), cover and management factor (USLE_C), and soil erodibility factor (USLE_K). Channel-related sediment processes are influenced by linear re-entrainment parameters (SPCON), the exponent for sediment re-entrainment (SPEXP), and the peak-flow adjustment factor for sediment routing (PRF), along with additional parameters controlling channel erosion such as the channel erodibility factor (CH_EROD) and channel cover factor (CH_COV1). Among these, PRF, SPCON, and SPEXP typically exert the strongest control on simulated sediment concentrations and therefore represent the most sensitive parameters during calibration.

2.6. Climate Change Scenarios

This study employs climate projections from the Coupled Model Intercomparison Project Phase 6 (CMIP6) to assess future climate scenarios in the Jordan Valley. It utilizes three Global Climate Models (GCMs): EC-Earth3-CC (Europe), HadGEM3-GC31-LL (UK), and MPI-ESM1-2-LR (Germany), under two Shared Socioeconomic Pathways (SSPs)—SSP2-4.5 and SSP5-8.5, representing medium and high greenhouse gas concentration trajectories. EC-Earth3-CC offers a comprehensive representation of the Earth system, HadGEM3-GC31-LL provides high-resolution simulations widely used in impact studies, and MPI-ESM1-2-LR delivers detailed large-scale dynamics [44–46]. Collectively, these models span a range of spatial resolutions and climate sensitivities, forming a robust ensemble for impact assessment in the Jordan Valley. The spatial distribution of grid points from the three models relative to the study watershed is shown in Figure S1 (Supplementary Information), highlighting resolution differences among them.

Daily precipitation and temperature series from the GCMs were bias-corrected before use in hydrological and geochemical simulations with SWAT. For precipitation, bias correction followed a four-step, trend-preserving workflow combining the Local Intensity–Occurrence (LOCI) method [47] and Quantile Delta Mapping (QDM) [48]. First, LOCI was applied on a monthly basis to the historical precipitation series to adjust wet-day frequency, aligning simulated and observed wet days (>0.1 mm d^{-1}) and reducing drizzle bias. Second, monthly QDM, using 201 quantiles with safe-tail extrapolation, was applied to historical and future precipitation amounts to correct precipitation while preserving climate change signals and realistic extremes. Third, a month-wise adjustment was applied to the corrected future precipitation series to preserve the raw model's projected change in wet-day frequency relative to the historical period. Fourth, a final change-locking step was applied so that corrected future mean precipitation changes for the analysis windows 2015–2050 and 2051–2095, relative to the 2000–2012 baseline, remained equal to the corresponding raw model percentage changes.

Post-correction evaluation focused on hydrologically relevant properties of the corrected precipitation series, including consistency of monthly wet-day frequency after occurrence correction, comparison of corrected historical precipitation against observations over the overlapping calibration period, and verification that the final corrected future series preserved the raw model's mean percentage change relative to the baseline period. For temperature (Tmin and Tmax), additive QDM with monthly safe-tail extrapolation was applied to align modeled and observed distributions while retaining projected shifts. A final additive change-locking step ensured that mean temperature changes (°C) for each period remained consistent with raw model outputs. The resulting bias-corrected datasets provided trend-preserving climate inputs for SWAT-based impact assessments under both emission scenarios.

3. Results

3.1. Model Setup and Basin Characteristics

The SWAT model was implemented for the Jordan Valley basin using the dominant HRU option. The watershed was delineated into 61 subbasins, each represented by a single dominant hydrologic response unit (61 HRUs in total), covering a total area of 422,516 ha. The dominant HRU option (one HRU per subbasin) was selected to reduce parameter dimensionality and support calibration under strong data limitations; we note, however, that this configuration aggregates within-subbasin land use, soil, slope, and management heterogeneity and may bias subbasin-scale nutrient, sediment, and irrigation estimates. The basin spans three administrative regions, with approximately 215,916 ha in Jordan, 75,092 ha in Israel, and 131,509 ha in Palestine. Land use within the basin is dominated by agricultural areas (49.5%), followed by barren land (17.8%), shrubland/semi-natural vegetation (15.9%), and pasture (15.4%), while forest, rangeland, urban, and open water areas together account for less than 2% of the total basin area. These percentages reflect the dominant HRU representation used in the SWAT model and are derived from the Land Use/Soil/Slope Distribution report for the delineated watershed. The modeled watershed includes a larger share of irrigated agricultural land compared to the broader Jordan Valley region.

The basin is characterized by predominantly steep terrain, with 57.9% of the area exhibiting slopes greater than 10%, 26.7% between 3 and 10%, and 15.4% below 3%. Soil information was derived from the Harmonized World Soil Database version 2.0 (HWSD v2.0). The dominant soil mapping units are s6687 (Calcaric Cambisols, 23.3%), s3560 (Fluvisols, 17.4%), s3532 (Chromic Luvisols, 17.3%), s3502 (Vertic Cambisols/Vertisols, 14.1%), and s3571 (Calcisols, 12.8%), which together account for more than 85% of the

watershed area. Soil classes are reported based on HWSD v2.0 mapping units and should be interpreted as indicative of dominant soil properties rather than site-specific classifications.

Daily meteorological forcing for the SWAT simulations was based on observed precipitation and air temperature time series covering the period 2000–2021. Precipitation inputs were obtained from 11 rainfall stations distributed within and around the Jordan Valley basin, allowing for a representative characterization of the spatial variability of rainfall across the watershed. Daily air temperature data were derived from 12 temperature stations, providing consistent coverage of the basin and its surrounding regions. All meteorological stations provided continuous records for the period 2000–2021 and were directly used as model inputs, with temperature values spatially interpolated by SWAT to the subbasin level.

3.2. Hydrologic Modeling with SWAT

The SWAT simulations reproduced the hydrological dynamics of the Jordan Valley across all monitored stations (Figure 2). Calibration was based on 22 hydrological parameters (Supplementary Table S1). Overall, the calibrated model reproduced the mean annual and seasonal discharge patterns across the watershed, despite uncertainties associated with dam operations, abstractions, and diversions. Although performance in a few subbasins—particularly Yavneal and Tavor—was affected by limited and potentially faulty observed data, simulated flows preserved the overall magnitude and temporal patterns of discharge in these basins. A formal split-sample calibration–validation approach was not feasible because discharge observations at most hydrometric stations were limited to relatively short and discontinuous time series, often covering only a few years. Instead, calibration was conducted for sub-basins with sufficient data availability, and the resulting parameter sets were subsequently transferred to hydrologically similar neighboring sub-basins. Model consistency was then assessed by evaluating simulated flows at downstream control points, particularly at the basin outlet, thereby providing a downstream consistency check of the transferred parameterization rather than an independent validation.

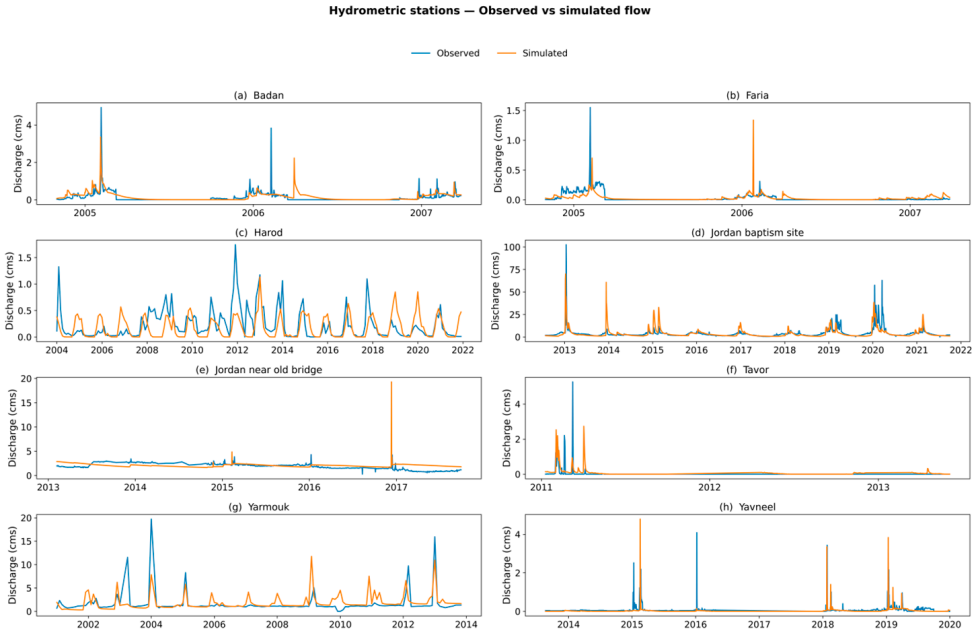

Figure 2. Observed (blue) and SWAT-simulated (orange) daily streamflow at eight hydrometric stations in the Jordan Valley basin (**a**–**h**). Discharge is shown in cubic meters per second ($m^3\ s^{-1}$).

At the Yavneal Hydrometric Station, surface runoff and soil hydraulic conductivity were identified as key controlling factors. At the Tavor Station, parameter transfer from Harod yielded flow patterns matching the observed (Figure 2). At the Jordan Near Old Bridge Station, model performance yielded a PBIAS of 6.7%, where both soil and channel parameters exerted a dominant influence on streamflow variability.

The Harod Station required explicit representation of aquaculture discharges as point sources to reproduce the observed seasonal flow regime. Following these adjustments, calibration yielded KGE = 0.4 and PBIAS = 21%. The observed Yarmouk discharge record includes two very high peaks (2003 and 2004) that are not explained by the available precipitation observations used in this study, and corresponding operational records (e.g., dam releases) were not available. Because their origin could not be independently resolved, these two events were excluded from the station-specific calibration assessment as a pragmatic screening step under unresolved observational/operational uncertainty, rather than as confirmed measurement artifacts. Accordingly, Yarmouk performance metrics should be interpreted with caution. When not considering these two peaks, the simulated hydrograph for the Yarmouk hydrometric station agrees with the observed discharge, with KGE = 0.4, PBIAS = 13%, and NSE = 0.3. Downstream, the Faria (KGE = 0.33; PBIAS = 0.04%) and Badan (KGE = 0.32, PBIAS = 0.33%) stations also achieved mixed performance with acceptable bias representation and limited but informative KGE; these sub-basins were primarily influenced by soil properties, precipitation distribution, and channel hydraulics. Finally, at the Jordan Baptism Site near the basin outlet, the model reproduced annual flow dynamics at the Jordan Baptism Site with PBIAS = 3%, KGE = 0.55, log-NSE = 0.3, and R^2 = 0.3 (Figure 2).

The hydrologic budget of the basin for the period 2000–2021 indicates an average annual precipitation of 298.9 mm, derived from observed meteorological data used as input to force the SWAT model, representing the primary internal water input to the basin. In addition to precipitation, the basin receives irrigation water that is imported from external sources and applied exclusively to irrigated HRUs, based on regional agricultural statistics and water-use records. Detailed operational data on irrigation deliveries, seasonal reservoir releases, pumping schedules, and allocation constraints were not available for the study area. However, the main irrigation source categories were identified from regional water-use information, with irrigation represented as externally supplied surface water for Jordan and Palestine and, where applicable, support from deep aquifer abstractions in Jordan. In the model, irrigation was simulated using SWAT auto-irrigation, such that irrigation timing and application amounts were triggered by crop water requirements rather than prescribed from observed operational schedules. Model-simulated evapotranspiration (ET), in the irrigated model, amounts to 282.9 mm, which reflects the combined effect of precipitation-derived soil moisture and externally supplied irrigation water. The mean irrigation input applied to irrigated areas corresponds to an equivalent basin-average depth of 84.8 mm. To provide a basin-scale interpretation of internal versus externally supported water use, a precipitation-derived ET equivalent was estimated in post-processing by subtracting the basin-average external irrigation input from total simulated ET. This is a theoretical bookkeeping estimate at the basin scale and should not be interpreted as a source-resolved ET partition computed internally by SWAT. After explicitly removing this external irrigation contribution, the evapotranspiration attributable to precipitation alone is 198.1 mm, corresponding to 66.3% of annual precipitation.

Surface runoff contributes 16.5 mm (5.5%), while lateral flow accounts for 27.9 mm (9.3%), and return flow adds 33.7 mm (11.3%) to streamflow generation. Revap from the shallow aquifer contributes 34.1 mm (upward flux of groundwater to the soil driven by evapotranspiration demand), whereas 59.6 mm (19.9%) percolates below the root zone

as groundwater recharge, and deep aquifer recharge is minimal (0.6 mm). All remaining water balance components reported above (surface runoff, lateral flow, return flow, revap, and groundwater recharge) are derived from SWAT model simulations. Overall, after removing the irrigation component from ET, the corrected water balance shows that the basin is strongly ET-dominated, with a contribution to shallow groundwater recharge and relatively modest surface runoff. The analysis of hydrological variability reveals pronounced differences between wet and dry years. Within the period 2000–2021, the wettest year was 2003, when basin-average precipitation reached 399.6 mm, corresponding to approximately 1688 MCM over the basin. After subtracting the irrigation depth (86.6 mm) from total ET, the evapotranspiration attributable to precipitation alone was 235.7 mm (≈995.8 MCM), leaving a surplus of about 163.9 mm (≈692.5 MCM) available for runoff, recharge, and changes in storage. In contrast, the driest year was 2017, with precipitation of only 124.7 mm (≈526.8 MCM), while ET from precipitation remained at 148.0 mm (≈625.3 MCM), slightly exceeding the annual precipitation. This implies a net depletion of basin water storage of roughly 23.4 mm (≈98.9 MCM) and effectively no surplus water for streamflow or recharge in that year. These results show pronounced differences in basin-scale water balance components between years with high precipitation (2003) and low precipitation (2017).

3.3. Geochemical and Sediment Transport Modeling Results

Annual livestock-derived nitrogen loads were calculated by multiplying animal population sizes by the corresponding nitrogen excretion rates and summing across all categories (Table 1). Livestock population data were obtained from national agricultural institutions in Israel, Palestine, and Jordan, corresponding to the most recent available statistics for the study period (2020–2021). Manure application was spatially restricted to sub-basins with slopes below 10%, reflecting common agricultural practices.

Table 1. Livestock nitrogen load by region and animal category.

Region	Animal Category	Number of Animals	N Excretion per Head (kg N/Head/yr)	Total N (t N/yr)
Jordan	Dairy cattle	47,979	80	3838.3
Jordan	Sheep and Goats	3,056,211	10	30,562.1
Jordan	Poultry	28,029,564	0.5	14,014.8
		Total Jordan		48,415.2
Israel	Dairy cattle	58,304	80	4664.3
Israel	Sheep and Goats	54,740	10	547.4
Israel	Poultry	14,230,131	0.5	7115.1
		Total Israel		12,326.8
Palestine	Dairy cattle	10,994	80	879.6
Palestine	Horses	2948	74	218.2
Palestine	Sheep and Goats	417,579	10	4175.8
Palestine	Poultry	1,912,410	0.5	956.2
		Total Palestine		6229.7

Therefore, during calibration, a uniform scaling factor of 2.7 was applied to the effective livestock-derived nitrogen load represented in the model in order to reproduce the observed outlet nitrate concentration. This adjustment was applied to the modeled source term, while the species-specific excretion coefficients remained unchanged. We note that the livestock inventory used in the initial setup was conservative relative to recent official/public livestock statistics reported by, e.g., the Palestinian Central Bureau of Statistics/Ministry of Agriculture, and therefore likely underestimated the effective source term (e.g., [49]). Accordingly, the livestock-derived nitrogen input used in the final simulations should be interpreted as an effective calibrated load rather than a direct census-based inventory.

Agricultural fertilizer-derived nitrogen loads were estimated using crop-type distributions and cultivated areas combined with crop-specific nitrogen requirements obtained from published agronomic recommendations and large-scale nutrient assessments. The agronomic data and crop-specific nitrogen requirements correspond to the most recent available recommendations for the study period (2020–2021). Nitrogen demand for annual crops was calculated on a per-hectare basis, while requirements for perennial crops were converted from per-tree values to an areal basis using typical planting densities before aggregation. Summing nitrogen demand across all crop types yielded total annual fertilizer inputs (Table 2). Estimated irrigation demand amounted to 206 MCM for Jordan, 67.8 MCM for Israel, and 51.5 MCM for Palestine.

Table 2. Nitrogen fertilizer demand by region and crop/land use group.

Region	Crop/Land Use	Area (ha)	N Application Rate (kg N/ha/yr)	Total N (t N/yr)
Jordan	Citrus plantations	6428.9	80	514.3
Jordan	Olive plantations	337.1	80	27.0
Jordan	Crop–fodder/arable	37,942.33	80	3035.4
Jordan	Vineyards	650.2	80	52.0
	Total Jordan			3628.7
Israel	Citrus plantations	195.1	80	15.6
Israel	Olive plantations	731.8	80	58.5
Israel	Crop–fodder/arable	20,061.3	80	1604.9
Israel	Vineyards	275.1	80	22.0
	Total Israel			1701.0
Palestine	Citrus plantations	92.33	130	12.0
Palestine	Olive plantations	889.5	130	115.6
Palestine	Crop–fodder/arable	15,097.5	130	1962.7
	Total Palestine			2090.3

The SWAT model simulated nitrate dynamics along the Jordan River (Figure 3). At the Jordan Baptism Site, the observed mean nitrate concentration (39.5 mg L^{-1} NO_3^-) was reproduced by the model (39.3 mg L^{-1} NO_3^-; PBIAS = −0.8%). Under the adopted management assumptions, the simulated nitrogen budget showed that denitrification accounted for less than 2% of applied fertilizer N, and ammonia volatilization was below 0.1. Of the 256.9 kg N ha^{-1} applied, approximately 12.7 kg N ha^{-1} was taken up by crops,

while the remaining nitrogen was retained in the soil, primarily through conversion to organic nitrogen pools, with soil organic N increasing from 426.5 to 626.4 kg N ha^{-1}. We note that these nitrogen budget terms represent model-estimated basin-average outputs under the adopted management assumptions and outlet-constrained nitrate calibration and should not be interpreted directly as field-scale nitrogen use efficiency or independently validated source-specific nitrogen balances.

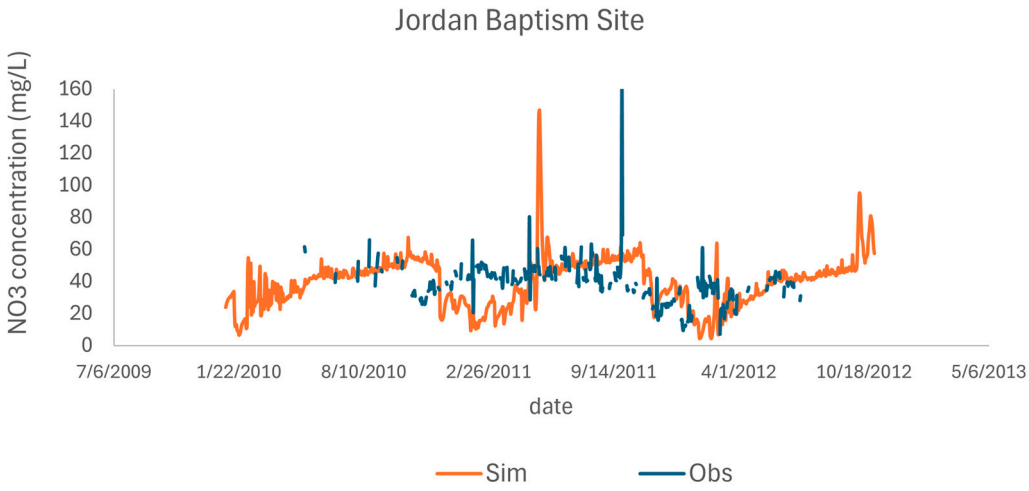

Figure 3. Observed (blue) and SWAT-simulated (orange) nitrate (NO_3^-) concentrations at the Jordan Baptism Site. Concentrations are shown in mg/L NO_3^-.

Sediment simulation at the Jordan Baptism Site (Figure 4) reproduced observed seasonal variability, with simulated concentrations of 2040 mg L^{-1} compared to observed values of 2200 mg L^{-1} (PBIAS = −8.1%; KGE = 0.6; NSE = 0.4; R^2 = 0.4). Spatial analysis identified steep sub-basins (slopes > 10%), particularly in the Yarmouk headwaters and parts of the West Bank, as dominant sediment source areas, with simulated erosion rates ranging from 29 to 219 Mg ha^{-1} yr^{-1}.

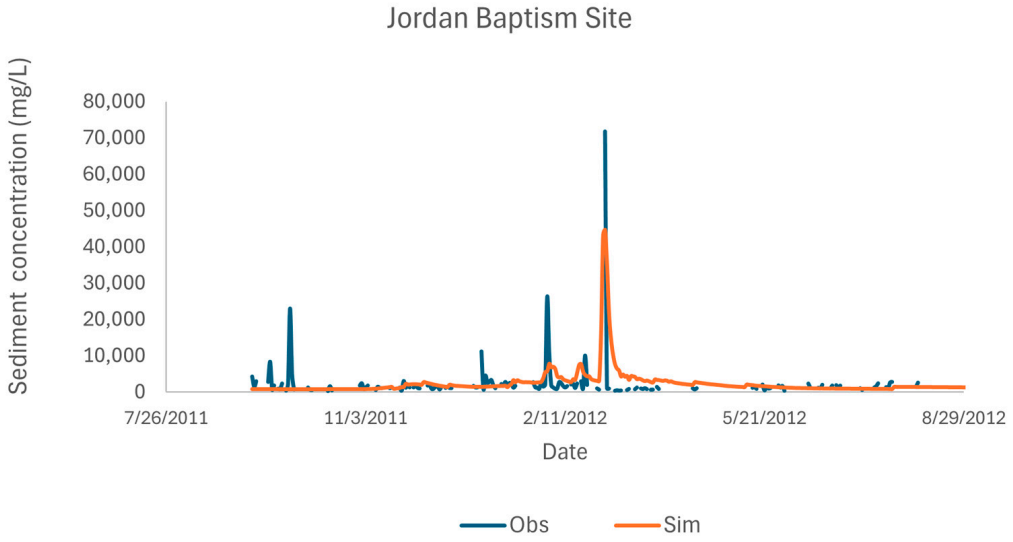

Figure 4. Observed (blue) and SWAT-simulated (orange) suspended sediment concentrations at the Jordan Baptism Site. Sediment concentrations are shown in mg/L.

3.4. Climate Change Scenarios Results

Supplementary Figures S2–S4 present precipitation model–observation comparisons and projections of maximum (Tmax) and minimum (Tmin) temperatures for Mid Ghor and North Ghor stations, representing the central and northern Jordan Valley. All three climate models—EC-Earth3-CC, HadGEM3-GC31-LL, and MPI-ESM1-2-LR—consistently project an increasing warming trend throughout 2020–2100, with higher magnitudes under SSP5-8.5. HadGEM3-GC31-LL exhibits the steepest rates of warming, occasionally exceeding +0.7 °C per decade, while MPI-ESM1-2-LR shows more moderate increases. Both Tmax and Tmin display similar upward trends in both daytime and nighttime temperatures across the region.

Projected hydrological components for 2020–2100 (Supplementary Figures S5–S8) reveal substantial changes in precipitation, evapotranspiration (ET), flow, and available water under both emission scenarios, with notable model-dependent differences. Precipitation exhibits pronounced interannual variability and a general tendency toward decline, particularly under SSP5-8.5, where all models simulate consistent decreases. These projections indicate reductions in freshwater inputs across the Jordan Valley.

Evapotranspiration projections display a predominantly declining trend across most models and scenarios. Model responses vary, with EC-Earth3-CC and HadGEM3-GC31-LL showing limited change under SSP2-4.5, while MPI-ESM1-2-LR indicates stronger reductions, particularly under high-emission conditions. The seasonal ET distribution (Supplementary Figure S6) remains characterized by spring–summer peaks followed by a pronounced dry-season decline.

River flow simulations (Supplementary Figure S7) suggest a gradual reduction across all scenarios, although with substantial interannual variability linked to precipitation fluctuations. Under SSP5-8.5, all models converge toward declining discharge and runoff, consistent with the anticipated reductions in rainfall and increased evaporative demand. Similarly, available water (Supplementary Figure S8) shows persistent decreases across most simulations.

The analysis of mean annual hydrological components (Tables 3–5) indicates substantial temporal variability in the projected water balance under both SSP2-4.5 and SSP5-8.5 scenarios for the periods 2020–2060 and 2060–2100. Under SSP2-4.5, most models suggest a moderate increase or stabilization of precipitation and available water towards the end of the century, accompanied by slight rises in evapotranspiration and river flow. Conversely, under the high-emission SSP5-8.5 pathway, precipitation and available water exhibit a marked decline after 2060.

Table 3. Summary of mean annual hydrological components (2020–2060 and 2060–2100) for EC-Earth3-CC (Europe) under SSP2-4.5 and SSP5-8.5 scenarios.

Scenario	Period	Precipitation (MCM/yr)	Available Water (MCM/yr)	Evapotranspiration (MCM/yr)	Flow (MCM/yr)
SSP2-4.5	2020–2060	1014.57	283.31	731.26	82.08
SSP2-4.5	2060–2100	1078.62	331.27	747.36	94.41
SSP5-8.5	2020–2060	1136.54	335.27	801.28	97.56
SSP5-8.5	2060–2100	988.00	276.29	711.71	78.75

Table 4. Summary of mean annual hydrological components (2020–2060 and 2060–2100) for HadGEM3-GC31-LL (UK) under SSP2-4.5 and SSP5-8.5 scenarios.

Scenario	Period	Precipitation (MCM/yr)	Available Water (MCM/yr)	Evapotranspiration (MCM/yr)	Flow (MCM/yr)
SSP2-4.5	2020–2060	1096.73	362.74	734	106.82
SSP2-4.5	2060–2100	1043.35	323.72	719.63	94.87
SSP5-8.5	2020–2060	1103.47	377.51	725.96	110.95
SSP5-8.5	2060–2100	1014.39	317.34	697.05	92.87

Table 5. Summary of mean annual hydrological components (2020–2060 and 2060–2100) for MPI-ESM1-2-LR (Germany) under SSP2-4.5 and SSP5-8.5 scenarios.

Scenario	Period	Precipitation (MCM/yr)	Available Water (MCM/yr)	Evapotranspiration (MCM/yr)	Flow (MCM/yr)
SSP2-4.5	2020–2060	1094.79	351.20	743.58	101.66
SSP2-4.5	2060–2100	950.88	271.41	679.47	75.23
SSP5-8.5	2020–2060	1100.06	356.23	743.83	104.10
SSP5-8.5	2060–2100	853.02	226.64	626.38	60.62

Historical mean hydrologic conditions for 2000–2020 were 1225 MCM yr^{-1} precipitation, 423 MCM yr^{-1} available water, 719 MCM yr^{-1} evapotranspiration, and 104 MCM yr^{-1} river flow. Supplementary Table S2 summarizes the projected percent changes relative to these baseline values. Under SSP2-4.5, precipitation is projected to decrease by 10–22%, with available water declining by up to 54%. Under SSP5-8.5, these reductions become more pronounced, reaching 30% for precipitation and 46% for available water during 2060–2100, while evapotranspiration remains relatively stable.

4. Discussion

The Jordan Valley represents a semi-arid and highly regulated basin where climatic variability and anthropogenic intervention jointly constrain water availability and quality. The overall model performance falls within the range typically considered satisfactory for first-order basin-scale interpretation under data-limited conditions, according to widely used evaluation criteria [34]. The adopted calibration strategy, including parameter transfer and downstream consistency assessment, is consistent with established SWAT applications and uncertainty approaches in data-scarce environments [33,38,39].

However, we note that model performance across the monitoring network was mixed, with relatively low NSE, log-NSE, and R^2 values at several stations. This indicates limited reliability for event-scale dynamics and local timing/magnitude in some sub-basins, particularly under strong regulation and incomplete operational data. Nevertheless, the model remains informative for first-order basin-scale interpretation and comparative scenario analysis. Accordingly, climate change projections are interpreted primarily as directional and relative signals rather than precise local forecasts, and water-quality results are considered more robust at the outlet-integrated scale than for detailed internal spatial attribution.

The basin water balance confirms a strongly evapotranspiration-dominated system. Even after excluding externally supplied irrigation water, evapotranspiration consumes the majority of precipitation-derived inputs. Such behavior is characteristic of semi-arid Eastern Mediterranean basins, where high atmospheric demand constrains renewable water availability [5,6]. The pronounced contrast between surplus conditions in wet years

and storage depletion in dry years reflects the high climatic sensitivity of the region and is consistent with previous assessments of climate impacts on Jordanian basins [1].

Human regulation plays a central role in shaping hydrological dynamics. Water diversions, reservoir operations, and transboundary allocation mechanisms have long been recognized as dominant controls in the Jordan River system [7,8,27]. Broader regional assessments also emphasize the structural influence of infrastructure and governance on water security in the Middle East [4,10]. The ability of the model to reproduce downstream discharge patterns despite limited operational data suggests that basin-scale water balance constraints are effectively represented over long-term averages.

Water quality simulations reveal a strong coupling between hydrology and nitrogen dynamics. Agreement at the Jordan Baptism Site indicates that the model reproduces outlet-integrated nitrate and sediment behavior, but it does not provide independent validation of upstream spatial gradients or source-area magnitudes. Nonetheless, the simulated spatial patterns remain physically plausible model-based inferences, reflecting topographic controls, land use, and the management assumptions applied in the model. In addition, because the livestock-derived nitrogen source term was partly adjusted during calibration to reproduce outlet nitrate concentrations, it should be interpreted as an effective modeled load rather than a directly observed inventory, with corresponding uncertainty in source attribution. The simulated nitrogen budget should also be interpreted with caution. The reported budget terms are basin-average model outputs aggregated across diverse crop systems and management practices, and SWAT partitions nitrogen among plant uptake, soil mineral and organic pools, and multiple loss pathways. Because fertilizer and manure application rates, timing, and spatial allocation are partly assumption-based under data limitations, the internal partitioning (including crop uptake versus applied N) is more uncertain than the outlet-integrated nitrate response. Therefore, the apparent low crop uptake should not be interpreted as a directly observed agronomic nitrogen use efficiency.

Previous hydrochemical investigations in the Lower Jordan River also identified agricultural return flows and groundwater contributions as key drivers of water quality degradation [13,14]. Earlier regional analyses also documented progressive water quality deterioration associated with diffuse agricultural inputs [2,12]. The dominance of diffuse agricultural sources and relatively low nitrogen uptake compared to applied inputs are consistent with global agricultural nitrogen balance assessments [40]. Under reduced discharge conditions, limited dilution capacity results in elevated in-stream concentrations, reinforcing previously observed discharge–concentration relationships in the Lower Jordan system [14].

Projected climate change impacts further intensify hydrological stress. Increasing temperatures and declining precipitation under high-emission scenarios are consistent with regional projections for the Eastern Mediterranean [5,6]. The projected reductions in available water correspond with previous modeling studies in semi-arid Jordanian basins [1]. Because evapotranspiration remains relatively stable compared to precipitation declines, future water deficits are likely to manifest primarily through reduced runoff and recharge, increasing structural water scarcity.

Uncertainties arise from the simplified representation of reservoir operations, the use of conceptual groundwater modules within SWAT [33], and inter-model variability among climate projections [44–46,48]. More broadly, recent hydrological modeling studies have shown that improving the representation of hydrological process heterogeneity can enhance both simulation realism and outlet performance, while also emphasizing the need to balance added process detail against model simplicity and available data; this tradeoff is directly relevant to the present basin-scale application, given the necessarily simplified HRU representation adopted here [50]. An additional source of uncertainty arises from

the reliability and comparability of published basin statistics in this politically and hydrologically complex transboundary setting. Reported values for infrastructure inventories, losses, and water transfers are drawn from secondary sources that differ in spatial scope, reporting year, and definitions, and in many cases cannot be independently verified against operational records. We therefore use these figures as contextual, order-of-magnitude indicators rather than precise constraints. Nevertheless, the internally consistent reproduction of discharge, nitrate, and sediment dynamics suggests that the framework captures the dominant hydrological and biogeochemical controls operating at the basin scale.

Beyond scientific interpretation, the results have direct practical relevance for water planning in the region. The clear separation between precipitation-derived water and externally supplied irrigation inputs highlights the structural dependence of the basin on regulated inflows and external allocations. This is particularly important in the context of the Jordan National Water Strategy 2023–2040 [30], which aims to enhance long-term water security under increasing climatic pressure. The projected reductions in available water suggest that maintaining current irrigation intensities and fertilizer application practices may become increasingly difficult without efficiency improvements. In this sense, the modeling framework developed here can function as a decision-support tool for evaluating alternative irrigation efficiencies, nutrient management strategies, and allocation scenarios within a transboundary WEFE nexus planning context [28,51].

Overall, the findings confirm that the Jordan Valley operates near its hydrological threshold, where modest climatic shifts or management changes may produce disproportionate system responses. Integrated modeling approaches that couple hydrology, nutrient transport, and human intervention provide an essential quantitative basis for adaptive management in transboundary and climate-stressed basins, complementing participatory WEFE nexus frameworks proposed for the region [28,51].

5. Conclusions

This study developed and applied an integrated hydrological and hydrogeochemical modeling framework to assess water availability and quality in the Jordan Valley, a heavily modified and data-limited transboundary basin. Despite limited information on reservoir operations, water abstractions, and diversions, the SWAT model satisfactorily reproduced the dominant hydrological behavior of the system and provided a consistent basin-scale water budget for the period 2000–2021.

The main conclusions of the study are summarized as follows:

The hydrological budget indicates that the Jordan Valley operates as a strongly evapotranspiration-dominated system. Mean annual precipitation amounts to 298.9 mm, of which 66.3% (198.1 mm) is lost through precipitation-derived evapotranspiration. When externally supplied irrigation water is included, total evapotranspiration increases to 282.9 mm, highlighting the strong dependence of agricultural activity on imported surface water and groundwater abstractions.

Internally available water resources are extremely limited, with only a small fraction of total water inputs contributing to river discharge toward the Dead Sea. This narrow water surplus places the basin close to its hydrological limits and makes it highly sensitive to both climatic variability and changes in upstream water management.

The hydrological response of the Jordan Valley is strongly controlled by human interventions, including dams, reservoirs, natural and artificial lakes, and transboundary diversions. Changes in upstream inflows are rapidly transmitted downstream, affecting river discharge along the Jordan River and inflows to the Dead Sea.

Given the mixed station-level performance and limited operational and water-quality observations, confidence is higher for basin-scale water-balance tendencies and comparative

scenario signals than for event-scale timing/magnitude at individual stations or detailed upstream water-quality source attribution.

Simulations of nitrate concentrations and sediment transport demonstrate a close coupling between hydrological conditions, land-use practices, and water quality. Low nitrogen use efficiency and elevated sediment yields in steep sub-basins indicate substantial pressures on both surface and groundwater resources, pressures that are likely to intensify under reduced flow conditions and declining dilution capacity. These inferences should nevertheless be interpreted with caution, as the spatial distribution and magnitude of internal nitrate and sediment source areas are influenced by management assumptions, coarse HRU representation, and the lack of independent upstream water-quality measurements.

Climate change projections consistently indicate a further reduction in water availability during the 21st century. Decreases in precipitation, river flow, and available water, particularly under high-emission scenarios, are expected to exacerbate existing water scarcity and increase stress on the hydrological system of the Jordan Valley.

This study is subject to several limitations that should be considered when interpreting the results. Reservoir operations and transboundary water transfers were represented in a simplified manner due to limited access to detailed operational records. Irrigation and domestic abstraction volumes were derived from available statistical reports and national datasets, which may not fully capture the spatial and temporal variability of actual withdrawals, particularly from groundwater sources. In addition, observed nitrate and sediment data were spatially and temporally limited, introducing additional uncertainty in the calibration of water quality simulations. Finally, uncertainty remains substantial due to limited and discontinuous streamflow records, parameter transfer across sub-basins, coarse HRU representation, incomplete operational data for regulation/diversions/irrigation, and outlet-focused water-quality calibration. Therefore, results are most reliable for basin-scale tendencies and comparative scenario analysis rather than fine-scale spatial attribution or event-scale prediction. These constraints should be taken into account when evaluating scenario-based projections.

Overall, the results indicate that the Jordan Valley is already operating close to its hydrological limits, where even relatively small changes in climate forcing or water management can lead to disproportionate impacts on water availability and quality. The modeling framework presented here provides a first-order basin-scale assessment framework for integrated hydrological assessments in heavily modified, data-constrained transboundary basins and supports future analyses under alternative climate and management scenarios.

Supplementary Materials: The following supporting information can be downloaded at https://www.mdpi.com/article/10.3390/w18060721/s1, Figure S1: Spatial distribution of climate model grid points (EC-Earth3-CC, HadGEM3-GC31-LL, and MPI-ESM1-2-LR) over the Jordan Valley Watershed; Figure S2: Annual Tmax and Tmin trends (2020–2100) for EC-Earth3-CC at Mid Ghor and North Ghor under SSP2-4.5 (blue) and SSP5-8.5 (red); Figure S3: Annual Tmax and Tmin trends (2020–2100) for HadGEM3-GC31-LL at Mid Ghor and North Ghor under SSP2-4.5 (blue) and SSP5-8.5 (red); Figure S4: Annual Tmax and Tmin trends (2020–2100) for MPI-ESM1-2-LR at Mid Ghor and North Ghor under SSP2-4.5 (blue) and SSP5-8.5 (red); Figure S5: Projected annual precipitation trends (2020–2100) under SSP2-4.5 and SSP5-8.5 scenarios for three climate models; Figure S6: Evapotranspiration trends (2020–2100) under SSP2-4.5 and SSP5-8.5 scenarios for three climate models; Figure S7: Annual hydrological flow trends (2020–2100) under SSP2-4.5 and SSP5-8.5 scenarios for three climate models; Figure S8: Available water projections (2020–2100) under SSP2-4.5 and SSP5-8.5 scenarios for three climate models; Table S1: QSWAT model parameters used for sensitivity analysis; Table S2: Percent decrease of precipitation, available water, ET and river flow from the 2000–2021 average hydrologic conditions.

Author Contributions: Conceptualization, N.P.N.; methodology, N.P.N.; formal analysis, A.M. and S.D.N.; software, S.D.N.; data curation, S.D.N., A.J., S.H., A.A., L.H., M.A.N., S.A.J. and D.E.; visualization, A.M.; writing—original draft, A.M.; writing—review and editing, A.M., S.D.N., A.J., S.H., A.A., L.H., M.A.L., M.A.N., S.A.J. and N.P.N.; supervision, N.P.N.; funding acquisition, N.P.N. All authors have read and agreed to the published version of the manuscript.

Funding: The authors declare that this study received funding from the European Union through the PRIMA Program, Grant Agreement No. 2243 (Project EcoFuture), Call 2022, Section 1: WEFE Nexus IA. The funder was not involved in the study design; collection, analysis, or interpretation of data; the writing of this article; or the decision to submit it for publication.

Data Availability Statement: The data presented in this study are available on request from the corresponding author due to restrictions from the data provider.

Acknowledgments: The authors acknowledge the support of collaborating institutions and stakeholders involved in data provision and consultation.

Conflicts of Interest: Author Suleiman Halasah was employed by the company Green Spectrum for Environmental Consulting, Amman, Jordan. The remaining authors declare that the research was conducted in the absence of any commercial or financial relationships that could be construed as a potential conflict of interest.

Abbreviations

The following abbreviations are used in this manuscript:

JV	Jordan Valley
SWAT	Soil and Water Assessment Tool
QSWAT	QGIS-based Soil and Water Assessment Tool interface
HRU	Hydrological Response Unit
DEM	Digital Elevation Model
ET	Evapotranspiration
GCM	Global Climate Model
CMIP6	Coupled Model Intercomparison Project Phase 6
SSP	Shared Socioeconomic Pathway
WEFE	Water–Energy–Food–Ecosystem Nexus
NSE	Nash–Sutcliffe Efficiency
KGE	Kling–Gupta Efficiency
PBIAS	Percent Bias
IMS	Israel Meteorological Service
PMD	Palestine Meteorological Department
WAJ	Water Authority of Jordan
FAO	Food and Agriculture Organization of the United Nations
HWSD	Harmonized World Soil Database
SRTM	Shuttle Radar Topography Mission
CFSR	Climate Forecast System Reanalysis
LOCI	Local Intensity–Occurrence method
QDM	Quantile Delta Mapping

References

1. Al-Bakri, J.; Suleiman, A.; Abdulla, F.; Ayad, J. Potential Impact of Climate Change on Rainfed Agriculture of a Semi-Arid Basin in Jordan. *Phys. Chem. Earth Parts A/B/C* **2011**, *36*, 125–134. [CrossRef]
2. Al Qatarneh, G.N.; Al Smadi, B.; Al-Zboon, K.; Shatanawi, K.M. Impact of Climate Change on Water Resources in Jordan: A Case Study of Azraq Basin. *Appl. Water Sci.* **2018**, *8*, 50. [CrossRef]
3. Food and Agriculture Organization of the United Nations. *The Future of Food and Agriculture—Trends and Challenges*; Food and Agriculture Organization of the United Nations: Rome, Italy, 2017.
4. World Bank. *Beyond Scarcity: Water Security in the Middle East and North Africa*; World Bank: Washington, DC, USA, 2017.

5. Lelieveld, J.; Hadjinicolaou, P.; Kostopoulou, E.; Chenoweth, J.; El Maayar, M.; Giannakopoulos, C.; Hannides, C.; Lange, M.A.; Tanarhte, M.; Tyrlis, E.; et al. Climate Change and Impacts in the Eastern Mediterranean and the Middle East. *Clim. Change* **2012**, *114*, 667–687. [CrossRef]
6. Zittis, G.; Almazroui, M.; Alpert, P.; Ciais, P.; Cramer, W.; Dahdal, Y.; Fnais, M.; Francis, D.; Hadjinicolaou, P.; Howari, F.; et al. Climate Change and Weather Extremes in the Eastern Mediterranean and Middle East. *Rev. Geophys.* **2022**, *60*, e2021RG000762. [CrossRef]
7. UN-ESCWA; Bundesanstalt für Geowissenschaften und Rohstoffe (BGR). *Inventory of Shared Water Resources in Western Asia*; United Nations Economic and Social Commission for Western Asia (UN-ESCWA): Beirut, Lebanon, 2013.
8. Gafny, S.; Talozi, S.; Al Sheikh, B.; Ya'ari, E. *Towards a Living Jordan River: An Environmental Flows Report on the Rehabilitation of the Lower Jordan River*; Friends of the Earth Middle East: Amman, Jordan, 2010.
9. Ministry of Water and Irrigation (MWI). *Annual Report on Water Resources and Uses in Jordan*; Ministry of Water and Irrigation: Amman, Jordan, 2021.
10. Kelley, C.P.; Mohtadi, S.; Cane, M.A.; Seager, R.; Kushnir, Y. Climate Change in the Fertile Crescent and Implications of the Recent Syrian Drought. *Proc. Natl. Acad. Sci. USA* **2015**, *112*, 3241–3246. [CrossRef]
11. Kool, J. *Sustainable Development in the Jordan Valley*; Hexagon Series on Human and Environmental Security and Peace; Springer International Publishing: Cham, Switzerland, 2016; Volume 13.
12. Salameh, E. *Water Quality Degradation in Jordan (Impacts on Environment, Economy and Future Generation Resources)*; Friedrich-Ebert-Stiftung: Berlin, Germany, 1996.
13. Farber, E.; Vengosh, A.; Gavrieli, I.; Marie, A.; Bullen, T.D.; Mayer, B.; Holtzman, R.; Segal, M.; Shavit, U. The Origin and Mechanisms of Salinization of the Lower Jordan River. *Geochim. Cosmochim. Acta* **2004**, *68*, 1989–2006. [CrossRef]
14. Hillel, N.; Geyer, S.; Licha, T.; Khayat, S.; Laronne, J.B.; Siebert, C. Water Quality and Discharge of the Lower Jordan River. *J. Hydrol.* **2015**, *527*, 1096–1105. [CrossRef]
15. Bergelson, G.; Nativ, R.; Bein, A. Salinization and Dilution History of Ground Water Discharging into the Sea of Galilee, the Dead Sea Transform, Israel. *Appl. Geochem.* **1999**, *14*, 91–118. [CrossRef]
16. Wu, Y.; Wang, W.; Toll, M.; Alkhoury, W.; Sauter, M.; Kolditz, O. Development of a 3D Groundwater Model Based on Scarce Data: The Wadi Kafrein Catchment/Jordan. *Environ. Earth Sci.* **2011**, *64*, 771–785. [CrossRef]
17. Alkhoury, W. Hydrological Modelling in the Meso-Scale Semiarid Region of Wadi Kafrein, Jordan—The Use of Innovative Techniques Under Data Scarcity. Ph.D. Thesis, Georg-August University of Göttingen, Göttingen, Germany, 2011.
18. Hoff, H.; Bonzi, C.; Joyce, B.; Tielbörger, K. A Water Resources Planning Tool for the Jordan River Basin. *Water* **2011**, *3*, 718–736. [CrossRef]
19. Al-Omari, A.; Al-Karablieh, E.; Al-Houri, Z.; Salman, A.; Al-Weshah, D.-R. Irrigation Water Management in the Jordan Valley under Water Scarcity. *Fresenius Environ. Bull.* **2015**, *24*, 1176–1188.
20. Al-Bakri, J.T.; D'Urso, G.; Batchelor, C.; Abukhalaf, M.; Alobeiaat, A.; Al-Khreisat, A.; Vallee, D. Remote Sensing-Based Agricultural Water Accounting for the North Jordan Valley. *Water* **2022**, *14*, 1198. [CrossRef]
21. Zhao, Z.; Cao, X.; Qin, G.; Zheng, Y.; Song, S.; Li, W. Coupled SWAT–MODFLOW Model for the Interaction Between Groundwater and Surface Water in an Alpine Inland River Basin. *Water* **2025**, *18*, 85. [CrossRef]
22. Wang, Y.; Zhang, K.; Luo, Y.; Zhang, Q.; Li, Z.; Yao, C.; Chen, X.; Wang, S.; Liu, J.; Zhang, C.; et al. GHydroMod-SIM-DAI v1.0: A New Distributed Hydrological Model Capable of Dynamically Recognizing Runoff Generation Mechanisms and Accounting for Aboveground and Underground Anthropogenic Impacts. *J. Hydrol.* **2025**, *663*, 134184. [CrossRef]
23. Meshesha, T.W.; Wang, J.; Melaku, N.D.; McClain, C.N. Modelling Groundwater Quality of the Athabasca River Basin in the Subarctic Region Using a Modified SWAT Model. *Sci. Rep.* **2021**, *11*, 13574. [CrossRef]
24. Mensah, J.K.; Ofosu, E.A.; Yidana, S.M.; Akpoti, K.; Kabo-bah, A.T. Integrated Modeling of Hydrological Processes and Groundwater Recharge Based on Land Use Land Cover, and Climate Changes: A Systematic Review. *Environ. Adv.* **2022**, *8*, 100224. [CrossRef]
25. El Harraki, W.; Zemzami, M. Assessing Climate Change's Impacts on Hydrology Using the SWAT Model: A Literature Review. *J. Water Clim. Change* **2025**, *16*, 1979–2005. [CrossRef]
26. Dai, H.; Yang, Y.; Zhang, F.; Guadagnini, A.; Yang, J.; Bu, X.; Wang, L.; Yuan, S.; Ye, M. Identification of Key Factors Driving Dissolved Oxygen in Riparian Aquifers Through Deep Learning-Assisted Global Sensitivity Analysis. *Water Resour. Res.* **2026**, *62*, e2025WR041884. [CrossRef]
27. Molle, F.; Mollinga, P.; Wester, P. Hydraulic Bureaucracies and the Hydraulic Mission: Flows of Water, Flows of Power. *Water Altern.* **2009**, *2*, 328–349.
28. Biggs, E.M.; Bruce, E.; Boruff, B.; Duncan, J.M.A.; Horsley, J.; Pauli, N.; McNeill, K.; Neef, A.; Van Ogtrop, F.; Curnow, J.; et al. Sustainable Development and the Water–Energy–Food Nexus: A Perspective on Livelihoods. *Environ. Sci. Policy* **2015**, *54*, 389–397. [CrossRef]

29. Jreisat, K.; Yazjeen, T. A Seismic Junction. In *Atlas of Jordan: History, Territories and Society*; Ababsa, M., Ed.; Contemporain Publications; Presses de l'Ifpo: Beyrouth, Lebanon, 2013; pp. 47–59.
30. Ministry of Water and Irrigation (MWI). *Jordan National Water Strategy 2023–2040*; Ministry of Water and Irrigation: Amman, Jordan, 2023.
31. Ibrahim, K.; Makhlouf, I.; El Naqah, A.; Al-Thawabteh, S. Geochemistry and Stable Isotopes of Travertine from Jordan Valley and Dead Sea Areas. *Minerals* **2017**, *7*, 82. [CrossRef]
32. Saha, S.; Moorthi, S.; Pan, H.-L.; Wu, X.; Wang, J.; Nadiga, S.; Tripp, P.; Kistler, R.; Woollen, J.; Behringer, D.; et al. The NCEP Climate Forecast System Reanalysis. *Bull. Am. Meteorol. Soc.* **2010**, *91*, 1015–1058. [CrossRef]
33. Arnold, J.; Moriasi, D.; Gassman, P.; Mikayilov, F.; White, M.; Srinivasan, R.; Santhi, C.; Harmel, R.; van Griensven, A.; Van Liew, M.; et al. SWAT: Model Use, Calibration, and Validation. *Trans. ASABE* **2012**, *55*, 1491–1508. [CrossRef]
34. Moriasi, D.N.; Arnold, J.G.; Van Liew, M.W.; Bingner, R.L.; Harmel, R.D.; Veith, T.L. Model Evaluation Guidelines for Systematic Quantification of Accuracy in Watershed Simulations. *Trans. ASABE* **2007**, *50*, 885–900. [CrossRef]
35. NASA Jet Propulsion Laboratory (JPL). *Shuttle Radar Topography Mission; (SRTM) GL1*; NASA Jet Propulsion Laboratory (JPL): Pasadena, CA, USA, 2013.
36. Food and Agriculture Organization of the United Nations (FAO). *Global Land Cover-SHARE (GLC-SHARE)*; FAO: Rome, Italy, 2014.
37. FAO; IIASA. *Harmonized World Soil Database Version 2.0*; FAO: Rome, Italy; International Institute for Applied Systems Analysis (IIASA): Laxenburg, Austria, 2023; ISBN 978-92-5-137499-3.
38. Abbaspour, K.C.; Johnson, C.A.; Van Genuchten, M.T. Estimating Uncertain Flow and Transport Parameters Using a Sequential Uncertainty Fitting Procedure. *Vadose Zone J.* **2004**, *3*, 1340–1352. [CrossRef]
39. Abbaspour, K.C.; Yang, J.; Maximov, I.; Siber, R.; Bogner, K.; Mieleitner, J.; Zobrist, J.; Srinivasan, R. Modelling Hydrology and Water Quality in the Pre-Alpine/Alpine Thur Watershed Using SWAT. *J. Hydrol.* **2007**, *333*, 413–430. [CrossRef]
40. Bouwman, A.F.; Lee, D.S.; Asman, W.A.H.; Dentener, F.J.; Van Der Hoek, K.W.; Olivier, J.G.J. A Global High-resolution Emission Inventory for Ammonia. *Glob. Biogeochem. Cycles* **1997**, *11*, 561–587. [CrossRef]
41. Intergovernmental Panel on Climate Change (IPCC). *Climate Change 1995: The Science of Climate Change*; Cambridge University Press: Cambridge, UK, 1995; ISBN 978-0-521-56436-6.
42. Organisation for Economic Co-operation and Development (OECD). *OECD Environmental Indicators for Agriculture*; OECD Publishing: Paris, France, 2007; Volume 4.
43. Food and Agriculture Organization of the United Nations (FAO). Emissions. In *Agriculture: Towards 2010*; FAO: Rome, Italy, 1995.
44. Döscher, R.; Acosta, M.; Alessandri, A.; Anthoni, P.; Arsouze, T.; Bergman, T.; Bernardello, R.; Boussetta, S.; Caron, L.-P.; Carver, G.; et al. The EC-Earth3 Earth System Model for the Coupled Model Intercomparison Project 6. *Geosci. Model Dev.* **2022**, *15*, 2973–3020. [CrossRef]
45. Andrews, T.; Andrews, M.B.; Bodas-Salcedo, A.; Jones, G.S.; Kuhlbrodt, T.; Manners, J.; Menary, M.B.; Ridley, J.; Ringer, M.A.; Sellar, A.A.; et al. Forcings, Feedbacks, and Climate Sensitivity in HadGEM3-GC3.1 and UKESM1. *J. Adv. Model. Earth Syst.* **2019**, *11*, 4377–4394. [CrossRef]
46. Mauritsen, T.; Bader, J.; Becker, T.; Behrens, J.; Bittner, M.; Brokopf, R.; Brovkin, V.; Claussen, M.; Crueger, T.; Esch, M.; et al. Developments in the MPI-M Earth System Model Version 1.2 (MPI-ESM1.2) and Its Response to Increasing CO_2. *J. Adv. Model. Earth Syst.* **2019**, *11*, 998–1038. [CrossRef]
47. Schmidli, J.; Frei, C.; Vidale, P.L. Downscaling from GCM Precipitation: A Benchmark for Dynamical and Statistical Downscaling Methods. *Int. J. Climatol.* **2006**, *26*, 679–689. [CrossRef]
48. Cannon, A.J.; Sobie, S.R.; Murdock, T.Q. Bias Correction of GCM Precipitation by Quantile Mapping: How Well Do Methods Preserve Changes in Quantiles and Extremes? *J. Clim.* **2015**, *28*, 6938–6959. [CrossRef]
49. Palestinian Central Bureau of Statistics; Ministry of Agriculture. *Joint Press Release on the Preliminary Results of the Agriculture Census, 2021*; PCBS: Ramallah, Palestine; MoA: Ramallah, Palestine, 2022.
50. Zhang, Q.; Zhang, K.; Bárdossy, A.; Li, Y.; Wu, N. Improving Representation of Hydrological Process Heterogeneity in Grid-Xin'anjiang Model through a Stepwise Approach. *J. Hydrol.* **2025**, *655*, 132897. [CrossRef]
51. Nikolaidis, N.P.; Troullaki, K.; Lilli, M.A.; Halasah, S.; Lehrer, D.; Rozakis, S.; Wald, S.; Al Ajrami, A.; Al-Attili, S.; Zemah-Shamir, S.; et al. An Integrated Participatory Framework for WEFE Nexus Strategic Planning: The Jordan Valley Case Study. *J. Environ. Manag.* **2025**, *375*, 124246. [CrossRef] [PubMed]